Changes in Modern Lifting-Line Methods for Swept Wings and Viscous Effects

Jose R. Chreim *, Marcos M. Pimenta†, and Gustavo R. S. Assi ‡
University of Sao Paulo, Sao Paulo, SP, 05508-900, Brazil

Joao L. D. Dantas§
Institute for Technological Research, Sao Paulo, SP, 05508-901, Brazil

A lifting-line formulation that makes possible the simulation of wings with sweep is presented; such formulation is based on modern adaptations of the classical theory and uses a nonlinear scheme to incorporate the influence of viscosity from real airfoil data on the wing lift and drag coefficients. The nonlinear scheme strictly satisfies the Pistolesi Boundary Condition over the control points at each iteration. The numerical accuracy of the method is verified through a standard procedure and the tool is consecutively validated against experimental data from several wings, each of which with a different planform. Satisfactory convergence rates, errors and uncertainties are obtained from the verification procedures and, for all wings, the agreement with experimental data are within a few percent. The results corroborate the reliability of the proposed formulation.

I. Nomenclature

b	=	wing span (m)
c_0	=	chord at the root of the wing (m)
C_c	=	axial section force coefficient
C_D	=	wing drag coefficient
C_L	=	wing lift coefficient
C_{LE}	=	extrapolated value of the numerical lift coefficient
C_{n_α}	=	slope of the $C_n \times \alpha$ curve $\left(\frac{\partial C_n}{\partial \alpha}\right)\left(\frac{1}{^\circ}\right)$
$C_{n_{\alpha_{Vis}}}$	=	slope of the viscous $C_n \times \alpha$ curve $\left(\frac{\partial C_n}{\partial \alpha}\right)\left(\frac{1}{^\circ}\right)$
$C_{n_{Pot}}$	=	'potential' normal section force coefficient
$C_{n_{Vis}}$	=	'viscous' normal section force coefficient
C_n	=	normal section force coefficient
C	=	constant of the function obtained with the Richardson Extrapolation
c	=	airfoil chord (m)
E_{h_a}	=	absolute error
E_{h_r}	=	relative error
F_s	=	safety factor of the Grid Convergence Index
$f(h_N)$	=	value of the function, obtained from the Richardson Extrapolation, at the representative grid size h_N
f_{ext}	=	extrapolated function value of the Richardson Extrapolation
GCI	=	Grid Convergence Index
h_N	=	representative grid size
i	=	control point/vortex index
j	=	control point/vortex index
k_j	=	index of the horseshoe vortex segment
k	=	constant of the numerical uncertainty

*MsC Candidate, Polytechnic School of the University of São Paulo, Av. Prof. Luciano Gualberto, Trav. 3, 380.
†Associate Professor, Polytechic School of the University of São Paulo, Av. Prof. Luciano Gualberto, Trav. 3, 380.
‡Associate Professor, Polytechic School of the University of São Paulo, Av. Prof. Luciano Gualberto, Trav. 3, 380.
§Research Engineer, Center for Mechanical, Naval and Electrical Technologies, Av. Prof. Almeida Prado, 532.

M_∞ = free-stream Mach number
M = section Mach number
$\mathbb{M}$ = influence matrix $\left(\frac{1}{m}\right)$
m = element of the influence matrix $\mathbb{M}$ $\left(\frac{1}{m}\right)$
N = number of horseshoe vortices
p = order of convergence of the Richardson Extrapolation
Re_∞ = free-stream Reynolds number
Re = section Reynolds number
$\vec{r}_{ij,k_j}$ = length vector from the k_j^{th} edge of the j^{th} horseshoe vortex to the i^{th} control point (m)
r = mesh refinement ratio
$\vec{u}_n$ = normal-to-the-planform unit vector
u_{num_a} = absolute numerical uncertainty
u_{num_r} = relative numerical uncertainty
$\vec{V}_{HS}$ = velocity induced by an entire horseshoe vortex $\left(\frac{m}{s}\right)$
$\vec{V}_{TV}$ = velocity induced by all the trailing vortices plus the free-stream velocity $\left(\frac{m}{s}\right)$
$\vec{V}_{VS}$ = velocity induced by a straight vortex segment $\left(\frac{m}{s}\right)$
$\vec{V}_\infty$ = free-stream velocity $\left(\frac{m}{s}\right)$
$\vec{V}$ = overall velocity at a control point $\left(\frac{m}{s}\right)$
$\vec{v}$ = auxiliary vector $\left(\frac{1}{m}\right)$
W_∞ = normal component of the free-stream velocity $\left(\frac{m}{s}\right)$
$\mathbf{W}_\infty$ = normal component of the free-stream velocity throughout the wing $\left(\frac{m}{s}\right)$
S_r = wing planform area $\left(m^2\right)$
x_{cp} = chordwise control point location (m)
y_{cp} = spanwise control point location (m)
z_{cp} = normal-to-the-planform control point location (m)
α_{eff} = wing section effective angle of attack $(^\circ)$
α = geometric angle of attack $(^\circ)$
α_{L0} = airfoil zero lift angle of attack $(^\circ)$
$\Delta\vec{F}$ = section aerodynamic force vector (N)
δ_A = planform area of the corresponding wing section $\left(m^2\right)$
$\vec{\delta}_l$ = bound vortex vector length (m)
Γ = circulation at a control point $\left(\frac{m^2}{s}\right)$
$\mathbf{\Gamma}$ = circulation distribution throughout the wing $\left(\frac{m^2}{s}\right)$
Λ = sweep angle $(^\circ)$
Ω = under relaxation factor
ρ = free-stream density $\left(\frac{kg}{m^3}\right)$
θ = angle between $\vec{V}_{VT}$ and $\vec{\delta}_l$ $(^\circ)$

II. Introduction

The conceptual aerodynamic design of wings is a phase that requires a balance between cost and accuracy: the aerodynamic tools used must provide reliable results relatively fast so as to cover a range variables of design. In this context, the selection of the appropriate tool is fundamental; while it cannot be too time consuming, its outputs must present errors within an engineering error acceptable range.

Among the various existing numerical methods, there is increasing interest in the so called *Computational Fluid Dynamics* (CFD) methods. They usually refer to numerical tools in which the flow field is specified through an Eulerian formulation and the physical domain is discretized using finite differences, finite elements, or finite volumes schemes. During the last decades, considerable advances in the application of CFD to the analysis and design of wings have been made; although CFD has not reached a fully confidence level, it is gradually gaining acceptance from academia and industry. Presently, however, these methods are limited in application due to the increased computational cost, the

reason they are often more interesting during the more advanced design phases.

On the other hand, modern lifting-line (LL) methods are a compromise between cost and accuracy. While not having the same level of detail as CFD, the current LL methods are still capable of predicting important features of the flow past wings; moreover, they are generally less computationally expensive, a feature that makes LL attractive for use during preliminary stages. These methods, however, evolved from simple potential flows to more sophisticated formulations in which viscosity and compressibility are considered on the wing design variables. In fact, current research in the field has even shown, for instance, that there is significant advantage in coupling LL with other numerical methods in order to reduce computational time of complex simulations [1].

Historically, the Lanchester-Prandtl's lifting-line was crucial to modern aerodynamics and brought insightful results that allowed several advances in wing design [2]; the original theory, however, is of limited application and the urge for wings with arbitrary geometries flying at high speeds have made the classical lifting-line gone through improvements in order to account for these needs [3].

Since its conception, several adaptations have been proposed to account for the effects of viscosity and the generality of wing geometries [4–13], among other interests. From the formulations proposed, Weissinger, using the earlier results of Pistolesi [14], developed a lifting-line for wings with arbitrary geometries: while the wing sections are represented by the usual $\frac{c}{4}$ line, the control points are placed along a $\frac{3c}{4}$ line, where the flow-tangency condition, more commonly known as *Pistolesi Boundary Condition* (PBC) is imposed [4]. With impressive results, Weissinger's lifting-line has later been widely used [5, 8, 9, 12, 13, 15].

The attempts to incorporate viscous effects on lift and drag, however, did not follow Weissinger's idea; while many authors used the '$\frac{c}{4} - \frac{3c}{4}$' representation, the accompanying nonlinear scheme usually used an equivalence between the potential lift (from the Kutta-Joukowski Theorem) and its viscous counterpart (from the definition of lift coefficient and the use of airfoil real data) as a requirement to correct Γ, leaving the PBC relaxed [9, 11, 13]. Moreover, the scheme generally needed a substantially low damping factor, so several hundred iterations were necessary for convergence [16].

Concomitantly to these attempts, a nonlinear scheme that strictly satisfied the PBC was proposed [17], and some works reported its implementation [16, 18]; the results from different authors were dissident, and no conclusion about the effectiveness of such could be drawn. Later and consequently, a novel scheme inspired on [17] was proposed [19] and it was reported to present adequate results; however, the lifting-line formulation of [19], used *horseshoe vortices* (HSV) that were not adequate for the imposition of the PBC. Thus, the author reported issues related to the convergence of the method.

Given the advantages of Weissinger's lifting-line for arbitrary geometries and its need to satisfy the PBC, and also the promising results of the nonlinear scheme proposed in [19], this work presents a nonlinear lifting-line formulation suitable for wings with sweep, in which the effects of viscosity on lift and drag are considered through airfoil data. In the next sections, a well-founded choice of the HSVs is presented followed by the formulation of the method. Next, code and solutions verifications are presented and the results show favorable convergence rates, errors, and uncertainties for all planforms evaluated. Validation of the method is performed against experimental data for four different wings and the small percentage difference substantiates the efficiency of the method for the proposed cases.

III. Choice of the Appropriate Horseshoe Vortex

For the current lifting-line formulation, three candidates for the horseshoe vortices (HSV) were assessed, and their geometries are presented on Fig. 1.

The HSV 'a' was initially adopted as it was used on previous works [21]. Although suitable for formulations in which the control point (CP) is placed over the bound vortex [10], this HSV does not work properly when the CP must satisfy the PBC: the circulation distribution becomes unstable and leads to divergence as the mesh is refined (Fig. 2). Such instability can be physically explained with the aid of Fig. 3, which presents the respective parts of the HSVs 'a' and 'b' that remain over the wing planform. For the sake of explanation, the HSVs have unitary circulation and the induced velocities are qualitatively represented by the numbered arrows; on a) the velocities induced by the segments over the spanwise outermost CPs are lower than over the innermost, implying that the final Γ distribution is higher at the tips. This effect increases with the angle of attack, as the free trailing vortices become less influential. If, instead, a trailing leg extends from the quarter chord-line to the trailing edge on each HSV, as on 'b', an additional contribution makes the velocity induced at the tips highly increase, while the increase near the root is not as intense. This makes Γ descreases towards the tips and improves numerical stability. (Fig. 4).

Therefore, between HSV 'a' and 'b', the second has been proven to be the appropriate. In comparison to HSV 'c', while there is no such straightforward advantage in using one over another, an important consideration about the

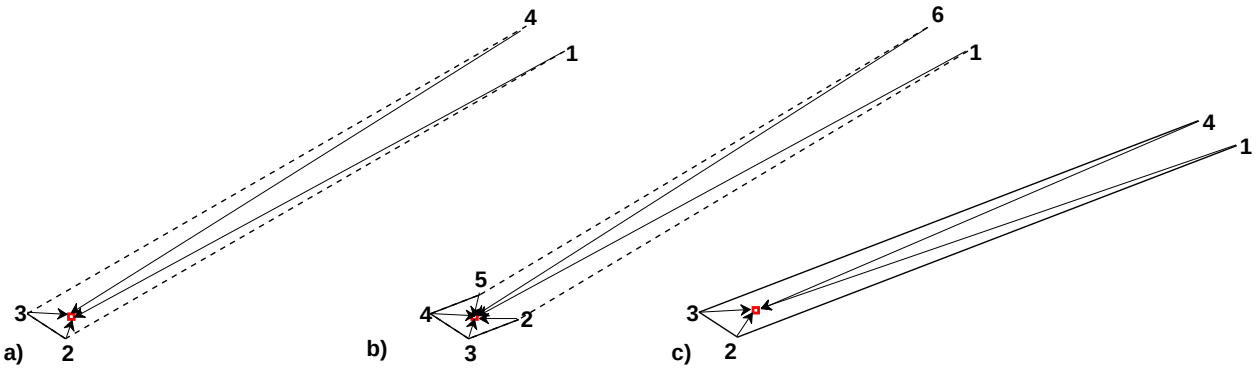

Fig. 1 Possible HSV models. a) The trailing vortices are shed into the free-stream direction from the bound vortex. b) Part of the trailing vortices remain over the planform, while the other part are shed into the free-stream direction. c) The trailing vortices are shed into the wing-planform-plane direction [20].

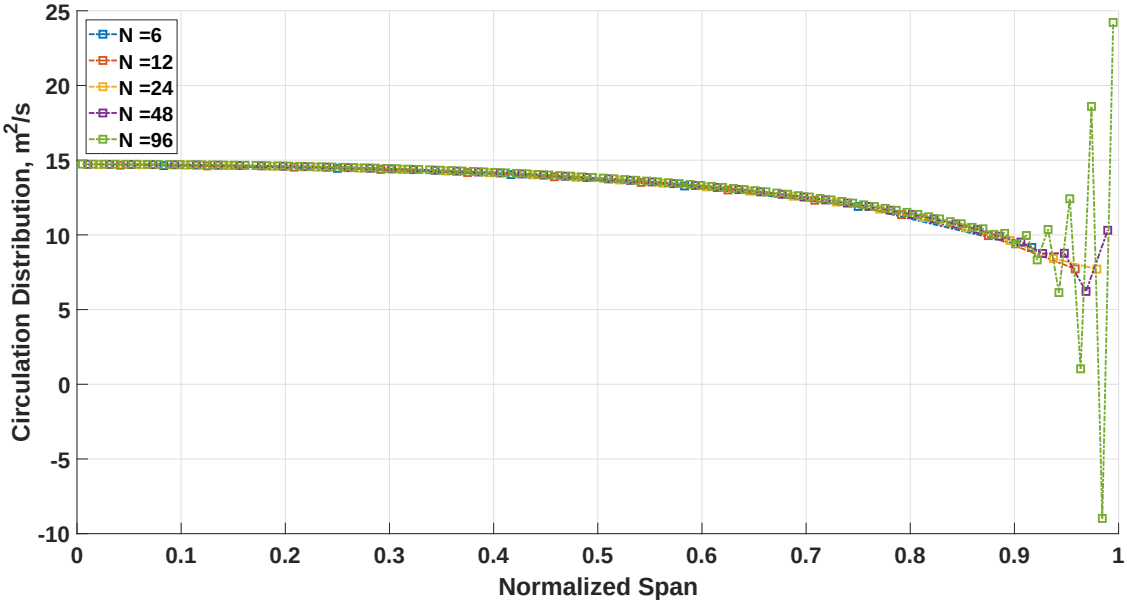

Fig. 2 Behavior of Γ as N is increased for the HSV 'a' of Fig. 1.

physics of the flow is that the trailing vortices must be shed into the flow towards the free-stream direction so that no aerodynamic forces act on them [20]. Although for very small α such consideration can be assumed to be true for HSV 'c', as the angle of attack increases this assumption can no longer be valid. Therefore, in order to correctly satisfy the physics behind the formulation, HSV 'b' was chosen as the singularity element.

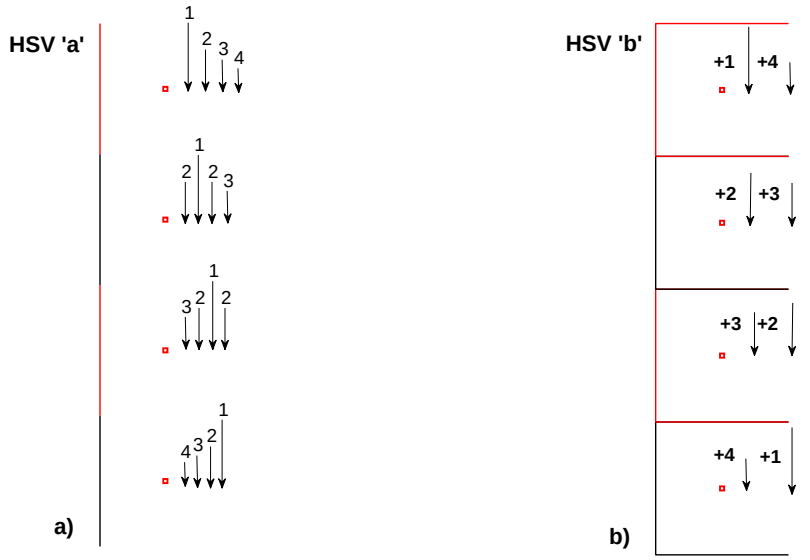

Fig. 3 Parts of the HSVs that stay on the wing planform regardless of the AoA. The arrows (from left to right) qualitatively represent the induced velocities of the HSVs (from top to down). The numbers represent the magnitude of the induced velocities at the specific CP (1 is the strongest).

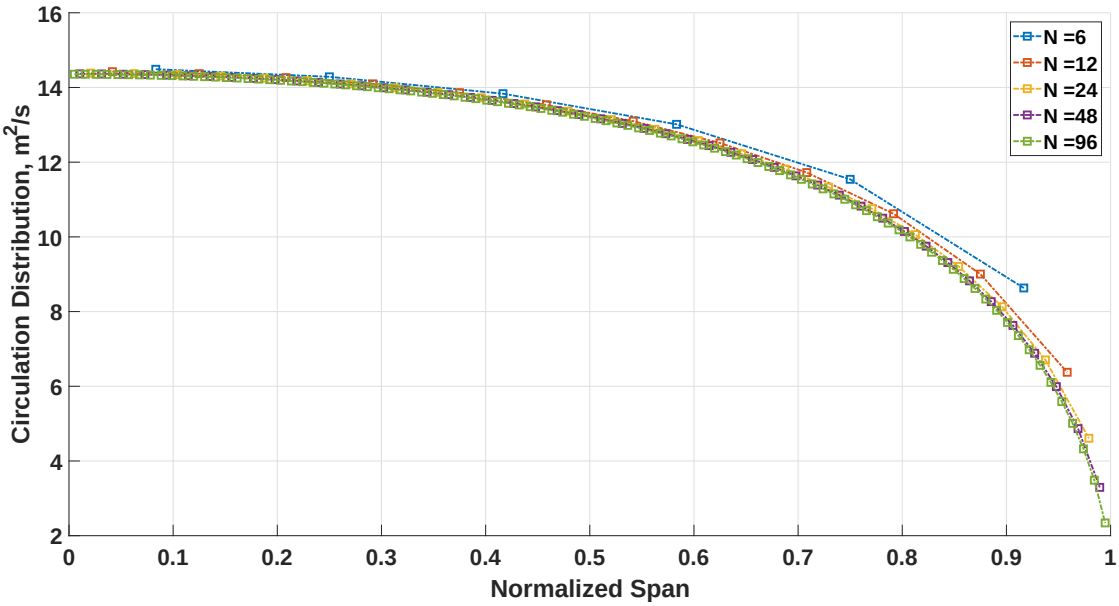

Fig. 4 Behavior of Γ as N is increased for the HSV 'b' of Fig. 1.

IV. Lifting-Line Formulation

Divided into linear and nonlinear schemes, the present lifting-line method is inspired on the works of [10, 19, 20]; the current formulation is suitable for wings with arbitrary quarter-chord lines, and it also accounts for the effects of viscosity on lift and drag up to stall region.

A. Linear Scheme

After defining the appropriate HSV, the wing and its wake are represented as depicted in Fig. 5: the *bound vortices* lay over the wing $\frac{c}{4}$ line, part of the *trailing vortices* remains over the wing planform, and the other part is shed towards the free-stream direction (into infinity). The velocity induced by a segment j (with vertices k_j and k_{j+1} and circulation Γ_j) over a point i can be analitically calculated with Eq. (1) [10, 20]:

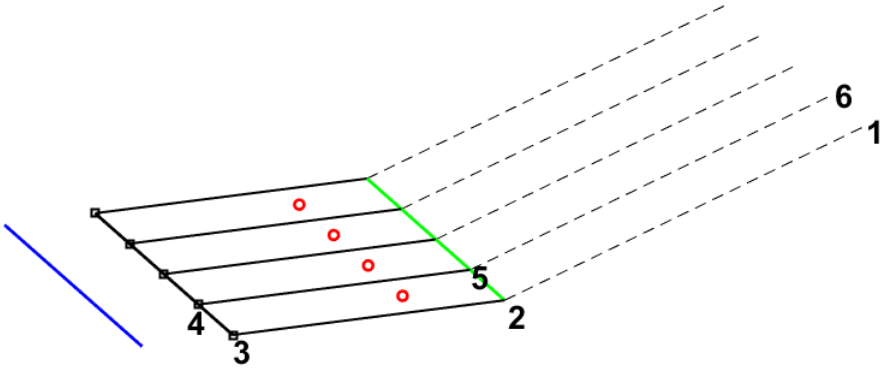

Fig. 5 Representation of the wing by a series of HSVs. For each HSV, the segment 2-3-4-5 remains over the wing planform, whereas the segments 1-2 and 5-6 are shed towards the free-stream.

$$\vec{V}_{VS_{ij,k_j k_j+1}} = \frac{\Gamma_j}{4\pi} \frac{\left(|\vec{r}_{ij,k_j}| + |\vec{r}_{ij,k_j+1}|\right)\left(\vec{r}_{ij,k_j} \times \vec{r}_{ij,k_j+1}\right)}{|\vec{r}_{ij,k_j}||\vec{r}_{ij,k_j+1}|\left(|\vec{r}_{ij,k_j}||\vec{r}_{ij,k_j+1}| + \vec{r}_{ij,k_j} \cdot \vec{r}_{ij,k_j+1}\right)} \tag{1}$$

such that the velocity of the entire horseshoe over i is given by the sum of all the individual contributions, according to the principle of superposition:

$$\vec{V}_{HS_{ij}} = \sum_{k_j=1}^{5} \vec{V}_{VS_{ij,k_j k_j+1}} = \frac{\Gamma_j}{4\pi}\vec{v}_{ij} \tag{2}$$

$$\vec{v}_{ij} = \sum_{k_j=1}^{5} \frac{\left(|\vec{r}_{ij,k_j}| + |\vec{r}_{ij,k_j+1}|\right)\left(\vec{r}_{ij,k_j} \times \vec{r}_{ij,k_j+1}\right)}{|\vec{r}_{ij,k_j}||\vec{r}_{ij,k_j+1}|\left(|\vec{r}_{ij,k_j}||\vec{r}_{ij,k_j+1}| + \vec{r}_{ij,k_j} \cdot \vec{r}_{ij,k_j+1}\right)} \tag{3}$$

The total velocity at i is the superposition of the velocity induced by the N HSVs and the free-stream velocity $\vec{V}_\infty$:

$$\vec{V}_i = \vec{V}_\infty + \sum_{j=1}^{N} \vec{V}_{HS_{ij}} \tag{4}$$

If the PBC is applied, the normal component of the velocity on Eq. (4) must be zero:

$$\vec{u}_{ni} \cdot \vec{V}_i = 0 \rightarrow \sum_{j=1}^{N} \vec{u}_{ni} \cdot \vec{V}_{HS_{ij}} = -\vec{u}_{ni} \cdot \vec{V}_\infty \tag{5}$$

Equation (5) can be more conveniently written with the aid of the rightmost expression of Eq. (2):

$$\sum_{j=1}^{N} m_{ij}\Gamma_j = -4\pi \times W_{\infty i} \tag{6}$$

$$m_{ij} = \vec{u}_{ni} \cdot \vec{v}_{ij}$$

$$W_{\infty i} = \vec{u}_{ni} \cdot \vec{V}_\infty$$

For each HSV there must be a corresponding control point (CP) at which the PBC is satisfied. Hence, Eq. (6) is imposed to the N CPs, and the resulting system of equations can be written in a matrix form:

$$\mathbb{M}\boldsymbol{\Gamma} = -\mathbf{W}_\infty \tag{7}$$

$\vec{\Gamma}$ can be obtained by solving Eq. (7), and the aerodynamic forces (and corresponding coefficients) are calculated considering only the influence of the trailing vortices [20]:

$$\vec{V}_{TVi} = \vec{V}_\infty + \sum_{j=1}^{N} \left(\vec{V}_{HS_{ij}} - \vec{V}_{VS_{ij,34}} \right) \tag{8}$$

$$\Delta\vec{F}_i = \rho\Gamma_i \vec{V}_{TVi} \times \vec{\delta}_{li} \rightarrow |\Delta\vec{F}_i| = \rho|\Gamma_i||\vec{V}_{TVi}||\vec{\delta}_{li}| \sin\theta_i \tag{9}$$

The Prandtl's hypothesis is assumed to be true and a three dimensional version of the *Kutta-Joukowski theorem* is used on Eq. (9) [10]. Finally, if $C_{n_{Poti}}$ is written as the definition of the 2-D normal force coefficient, an expression in terms of Γ_i is obtained:

$$C_{n_{Poti}} = \frac{|\Delta\vec{F}_i|}{\frac{1}{2}\rho|\vec{V}_{TVi}|^2\delta A_i} = \frac{|\Gamma_i||\vec{\delta}_{li}| \sin\theta_i}{\frac{1}{2}|\vec{V}_{TVi}|\delta A_i} \tag{10}$$

B. Nonlinear Scheme

In the present nonlinear scheme, viscosity is incorporated by moving the CP into the chordwise direction along the planform wing surface and imposing the PBC at the new location. This process effectively changes the coefficients m_{ij} and physically approximates the curves $C_{ni} \times \alpha_i$ and $C_{n_{Vis}i} \times \alpha_i$, as shown on Fig. 6.

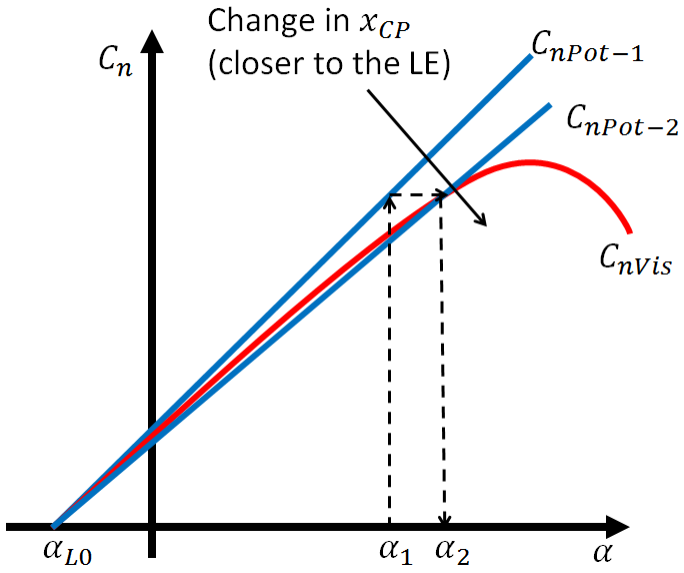

Fig. 6 Scheme for the nonlinear formulation. The control points chordwise locations determine the slopes of the curves C_{n_α}.

Originally, the PBC was derived under the assumption of a flat-plate airfoil [14], whose slope C_{n_α} is 2π; if a wing section is such that $C_{n_\alpha i} \neq 2\pi$, x_{cpi} must be changed accordingly to reflect the differences:

$$x_{cpi} = \frac{3}{4}\frac{C_{n_\alpha i}}{2\pi}c_i \tag{11}$$

y_{cpi} and z_{cpi} must be changed accordingly to ensure that the CP remains over the wing planform. The linear process is then repeated to obtain a new estimate for $C_{n_{Poti}}$; this step is necessary to ensure that PBC is satisfied for the new CP location. The effective angle of attack is then calculated with Eq. (12):

$$\alpha_{effi} = \frac{C_{n_{Pot}i}}{C_{n_\alpha i}} + \alpha_{L0i} \tag{12}$$

Viscosity is incorporated on lift by real airfoil data as a function of (α_{eff_i}), (M_i), and (Re_i). These data are generally obtained from experiments or numerical simulations and presented in terms of the airfoil aerodynamic normal force coefficient:

$$C_{n_{Vis}i} = C_{n_{Vis}}\left(\alpha_{effi}, M_i, Re_i\right) \quad . \tag{13}$$

$C_{n_{Vis}i}$ is compared with $C_{n_{Pot}i}$; if they do not agree to within a specified tolerance, a viscous $C_{n_\alpha i}$ is calculated from $C_{n_{Vis}i}$:

$$C_{n_{\alpha_{Vis}}i} = \frac{C_{n_{Vis}i}}{\alpha_{effi} - \alpha_{L0i}} \tag{14}$$

Equation (14) assumes that $C_{n_{\alpha_{Vis}}i}$ has a linear behavior; hence, the nonlinear formulation is only suitable until stall region. Finally, $C_{n_\alpha i}$ is updated according to Eq. (15):

$$C_{n_\alpha i} = \Omega C_{n_\alpha i} + (1-\Omega)\, C_{n_{\alpha_{Vis}}i} \tag{15}$$

Ω tipically assumes the value of 0.8. The nonlinear process is repeated until convergence is achieved. C_{ci} is concomitantly calculated through the same 2-D data. This coefficient, however, is not used on the iterative process, but only on the post-processing calculations, and it is related to the airfoil viscous drag contribution on the wing lift and drag; for inviscid cases $C_{ci} = 0$.

C. Lift and Drag Coefficients

The wing lift and drag coefficients are obtained from the values of C_n and C_c. For each of these values, a corresponding transformation, in terms of the geometric and the effective angles of attack (from local to global coordinates) must be performed.

$$C_L = \frac{1}{|\vec{V}_\infty|^2 S_r} \sum_{i=1}^{N} |\vec{V}_i|^2 \delta A_i \left[C_{n_i} \cos\left(\alpha - \alpha_{effi}\right) - C_{c_i} \sin\left(\alpha - \alpha_{effi}\right)\right] \tag{16}$$

$$C_D = \frac{1}{|\vec{V}_\infty|^2 S_r} \sum_{i=1}^{N} |\vec{V}_i|^2 \delta A_i \left[C_{n_i} \sin\left(\alpha - \alpha_{effi}\right) + C_{c_i} \cos\left(\alpha - \alpha_{effi}\right)\right] \tag{17}$$

As expected, the inclusion of viscous drag increases the overall drag whilst it decreases the lift.

D. Flowchart of the formulation

The following flowchart illustrates the method described in this section. The dashed lines represent the path the linear formulation takes, whereas the continuous ones, the path for the nonlinear formulation:

V. Results

According to the ASME V&V 20 Committee [22], validation is necessary to determine the accuracy of a given numerical method in representing the physics at which it has been intended. Prior to validation, however, code and solution verifications must be performed to any numerical method in order to ensure its reliability. Verifications were done by systematically refining the discretization and either observing the behavior of the numerical solution, or comparing it with theoretical results, when available. The theoretical result of the elliptical planform wing served as a benchmark for the verification of the linear formulation, whereas for the nonlinear two other geometries were used. For validation, the numerical results were compared to experimental data from the literature [23, 24].

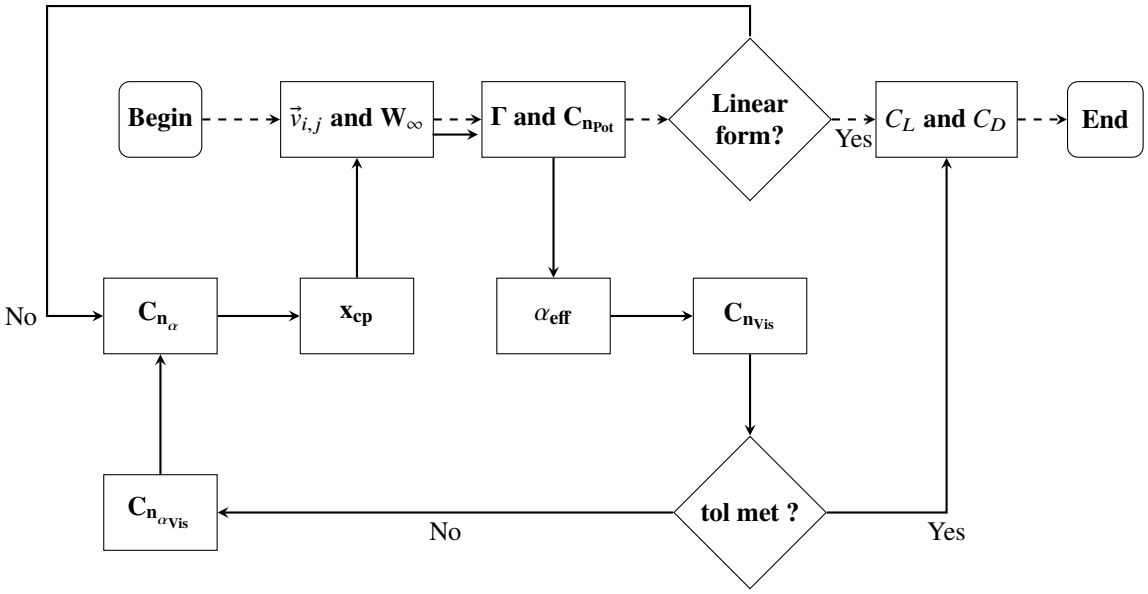

Fig. 7 Flowchart of the WLL indicating both linear and nonlinear schemes on the formulation and their interaction.

A. Code and Solution Verification

Both evaluation and estimation of the error were performed through the Richardson Extrapolation procedure; as systematic grid refinement was necessary, a family of grids with the coarsest half wing discretization having 28 elements and the finest one having 904 was constructed. The number of HSVs was consecutively increased by a ratio of approximately $\sqrt{2}$, a value recommended by the committee [22]. The number of elements was represented by a refinement ratio r, according to Eq. 18: $r = 1$ relates to the finest grid and $r = 0$ to an extrapolation in which N tends to infinity.

$$r = \frac{h_N}{h_{N_{Max}}} \quad . \tag{18}$$

For the present formulation, h_N assumed the definition of Eq. (19):

$$h_N = \frac{\sum_{i=1}^{N} |\vec{\delta}_{li}|}{N} \quad . \tag{19}$$

The behavior of the solution that is in the convergence region was assumed to follow Eq. (20); from the expression, fitting curves were plotted against r.

$$f(h_N) = f_{ext} + C h_N^p \tag{20}$$

Therefore, either E_{h_r} or E_{h_a} was evaluated simply by calculating the difference

$$E_{h_r} = |f_{ext} - f(h_N)|/|f_{ext}| \quad E_{h_a} = |f_{ext} - f(h_N)| \tag{21}$$

whereas the corresponding uncertainty (u_{num_r} or u_{num_a}) was estimated through a Grid Convergence Index (Eqns. 22 and 23):

$$GCI = \frac{F_S \times |f(h_{N_{max}}) - f(h_{(N_{max}-1)})|}{\left[\frac{h_{N_{max}}}{h_{(N_{max}-1)}}\right]^p - 1} \tag{22}$$

$$u_{num_r} = GCI/(k \times f_{ext}) \quad u_{num_a} = GCI/k \tag{23}$$

Table 1 Wings geometric properties.

Property	Case I	Case II	Case III
Wing Planform	Elliptical	Straight	Straight
Wing Section	Flat plate	NACA 0012	Flat plate
b (m)	2.0544	5.900	2.4892
c_0(m)	0.3566	1.00	0.5080
Λ (deg)	0	0	45

The assigned values for F_s and k were 1.25 and 1.1, respectively, so that a conservative uncertainty could be estimated. The characteristics of the three wings used as benchmarks are summarized on table 1 and their planforms are illustrated on Fig. 8. Furthermore, C_L was used as variable of comparison.

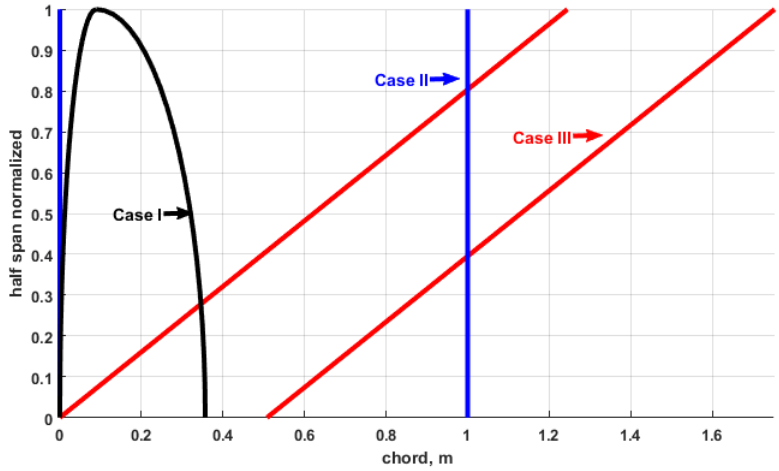

Fig. 8 Wing planforms for code and solution verifications: on each wing, the leading edge is the leftmost line.

Additionally, the literature reports evidence about the influence of the spanwise discretization on the rate of convergence; while in [20] it is suggested a spatial equispaced discretization for both the HSVs and the CPs, in [10] it is claimed that cosine clustering for both HSVs and CPs is preferred for its efficiency. The latter authors also claim that denser clustering is needed whenever there are discontinuities at the quarter-chord line, since rapid changes in Γ happen at these locations. Given the dissidence, three clustering schemes were evaluated: the equispaced (EHEP - Equidistant HSV, Equidistant CP), the cosine (CHCP - Cosine HSV, Cosine CP), and a combination in which the HSVs have a cosine distribution and the CPs are placed midway the trailing segments of the HSVs (CHEP - Cosine HSV, Equidistant CP). Figure 9 illustrates the three discretizations.

The flat-plate elliptical-planform wing (table 1, case I) was chosen due to the existence of theoretical solution under potential flow conditions [6]; the planform shape is also interesting to assess the method given the variable chord distribution. Figure 10 shows the numerical C_L as function of h_N and as a percentage of the theoretical value (the horizontal line at $C_L = 100\%$); a zoom in the convergence region is presented on the right plot, where both the extrapolated values and numerical uncertainties for the finest grids are highlighted. While the theoretical C_L is approximately 0.6599, for the EHEP and CHEP the C_{L_E} found were 0.6656 and 0.6655, respectively. The corresponding p were approximately and 1.05 and 0.98, values that indicate first order convergence accuracy, which is satisfactory, according to [22]. In terms of percentage difference, both C_{L_E} were approximately 0.08 % offset from the theory. Finally, for the CHCP no smooth convergence was observed with RE procedure, although it is evident from the figure that the trend for this clustering was better than for the two others; a different verification procedure is thus necessary in this case.

The NACA0012 straight-planform wing under viscous flow (table 1, case II) was chosen to evaluate the nonlinear scheme when effects of viscosity are incorporated. A straight planform wing was used to keep the variations in Re small throughout the wing, since large variations could lead to a possible source of error from the 2-D aerodynamic

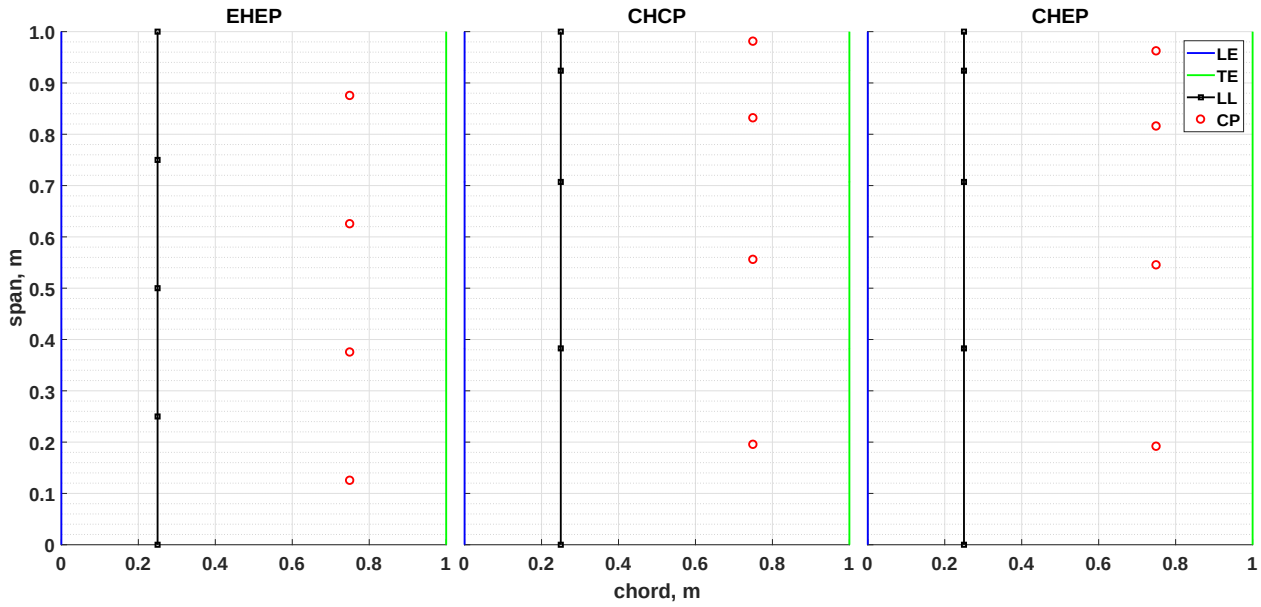

Fig. 9 Clusterings evaluated: EHEP, CHCP, and CHEP.

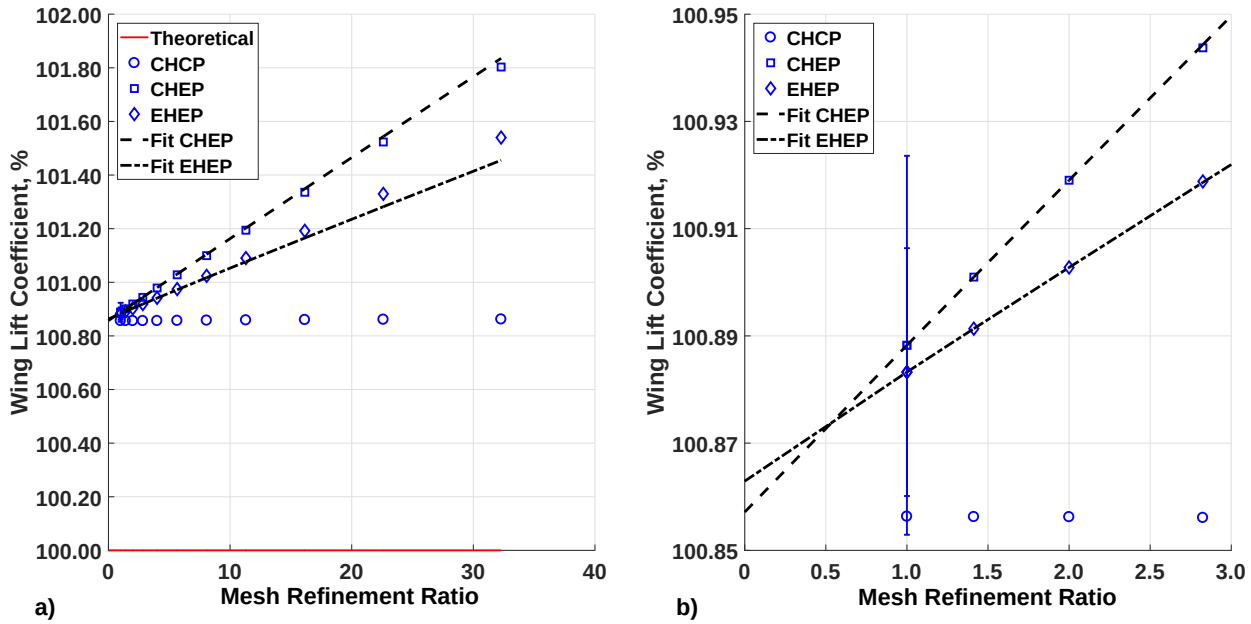

Fig. 10 a) C_L versus r for the elliptical wing under potential flow ($V_\infty \approx 74.68\ m/s,\ \alpha = 8°$, Case I). The symbols are the numerical C_L, the lines are the fitting curves obtained through RE, and the horizontal line at $C_L = 100\%$ is the theoretical solution. b) Zoom of the convergence region.

data. Once more, Fig. 11 shows the numerical C_L as the grid is refined, and the graph on the right is a zoom in the convergence region. The extrapolated lift coefficient and the rate of convergence were approximately 0.5972 and 1.00 for both EHEP and CHEP discretizations. No smooth convergence was observed for CHCP with RE, although it is clear again that it seemed to presented a better convergence behavior than the others.

Finally, the flat-plate 45°−sweptback wing under potential flow (table 1, case III) was chosen to assess the method

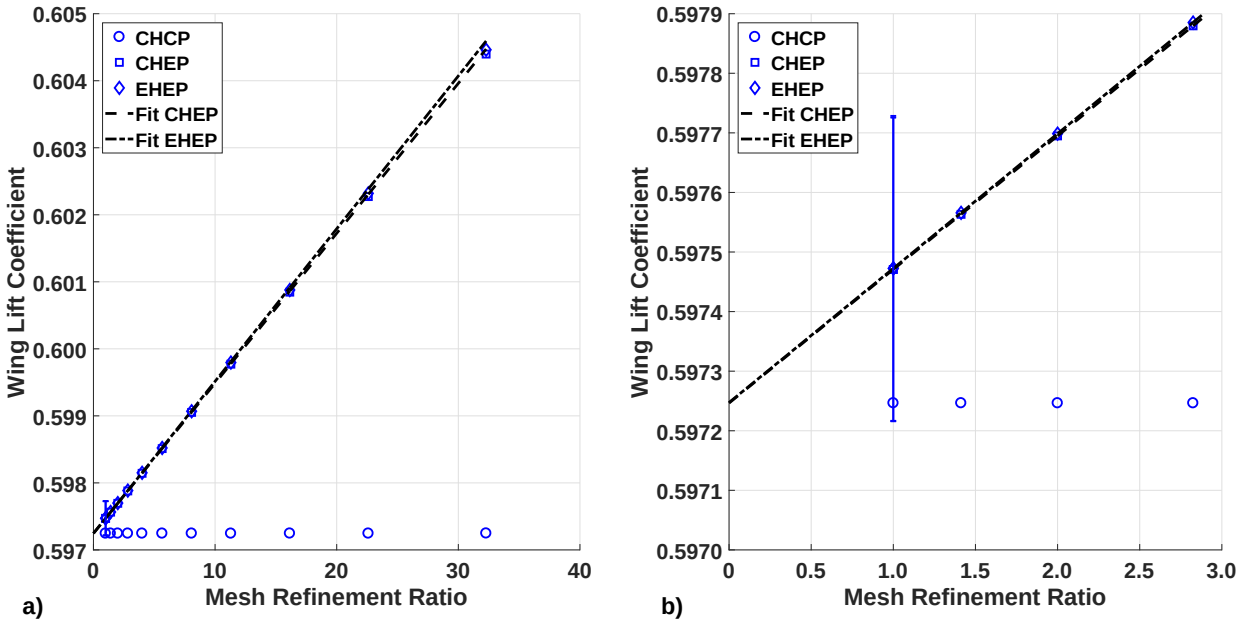

Fig. 11 a) C_L versus r for the straight wing under viscous flow ($V_\infty \approx 49.67\ m/s,\ \alpha = 8°$, Case II). The symbols are the numerical C_L, whereas the lines are the fitting curves obtained through RE. b) Zoom of the convergence region.

behavior when three dimensional effects are more intense. From Fig. 12, all C_{LE} were approximately 0.4502, and p for EHEP and EHCP were, correspondingly, 1.0024 and 0.9980. For this case, CHCP convergenced with the RE and, corroborating the expectations, p was significantly higher ($p \approx 2.00$), a value that indicates that the PLL converges at approximately the theoretical rate with this clustering; thus, the behavior of the solution in the convergence region is close to asymptotic.

B. Validation

The present lifting-line was validated against experimental data from the literature [23–25]. The discretization was set to 320 elements per semi-span. To have the same wing planform as reported in the experiment, for the elliptical wing, a straight rectangular inboard section segment is added, whereas both b and c_0 remain unchanged; therefore, for half span, in the spanwise direction from 0 to approximately 0.183 m the planform is straight, while from 0.183 m to 1.0272 m the planform follows an elliptical distribution (Fig. 16, case IV). The straight and sweptback wings remained the same.

For the elliptical wing, $Re_\infty \approx 2.11 \times 10^6$ with respect to c_0 (or 1.70×10^6 with respect to the mean aerodynamic chord) and $M_\infty \approx 0.27$. The experimental data are from [25]: boundary-layer transition mechanisms were placed along the wing span, at 5% of the chord (in the free-stream direction) over both the upper and the lower surfaces, so the flow was assumed to be turbulent; additionally, in most of the α range, the increment in the angle of attack was 0.5°. For the numerical simulations, the source of airfoil data was the Star-CCM+ Computational Fluid Dynamics (CFD) software: only C_n data were used, because the large variations in Re would require a more detailed study (related to turbulence models, for instance); therefore, since it is believed that the variations in C_c are small, a constant value of 0.01293 was assumed for all wing sections and simulated angles of attack.

In terms of the coefficients, the agreement is satisfactory over all the α range, apparently becoming subtly worse for higher angles of attack. Nevertheless, the differences are no higher than 2.2 % for both C_L and C_D, according to Fig. 13.

For the straight wing, $Re_\infty \approx 3.17 \times 10^6$ and $M_\infty \approx 0.15$. The experimental data are from [24]: turbulence was enforced at about 5 cm downstream the wing leading edge as to have an essentially turbulent flow. For the numerical method, the source of airfoil data was again the Star-CCM+. Figure 14 shows the trends for C_L and C_D as function of α. For both C_L and C_D, a satisfactory agreement happens between the current lifting-line and the experimental data in the

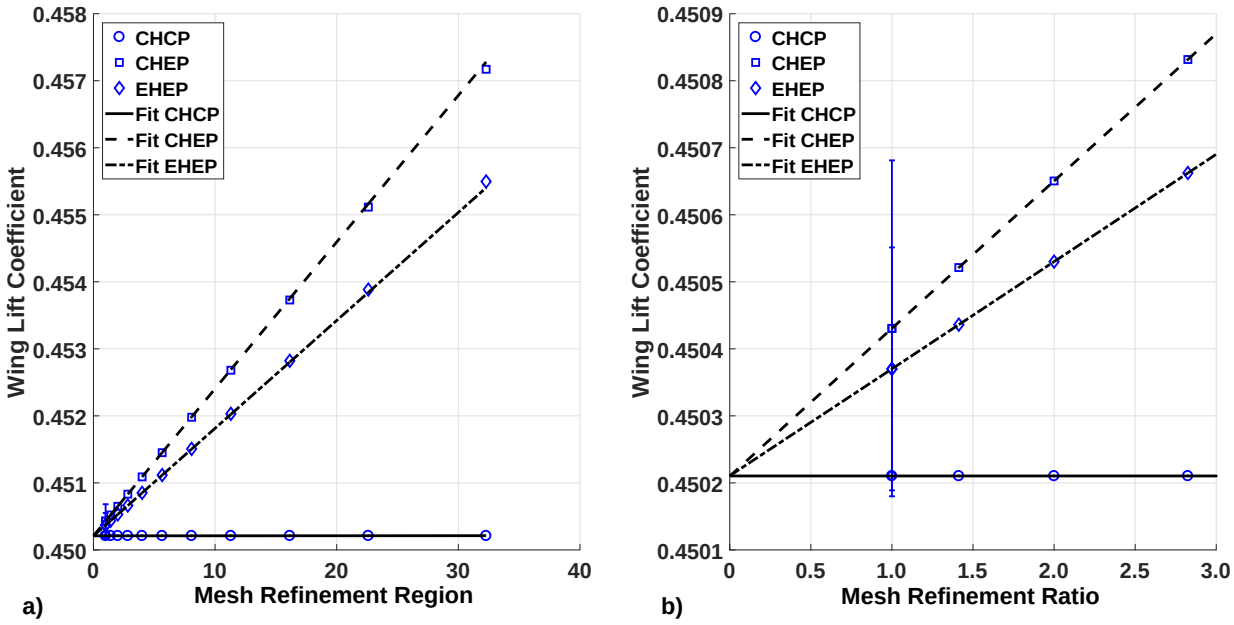

Fig. 12 a) C_L versus r for the $45°-$sweptback wing under potential flow ($V_\infty \approx 51.81\ m/s,\ \alpha = 8°$, Case III). The symbols are the numerical C_L, whereas the lines are the fitting curves obtained through RE. b) Zoom of the convergence region.

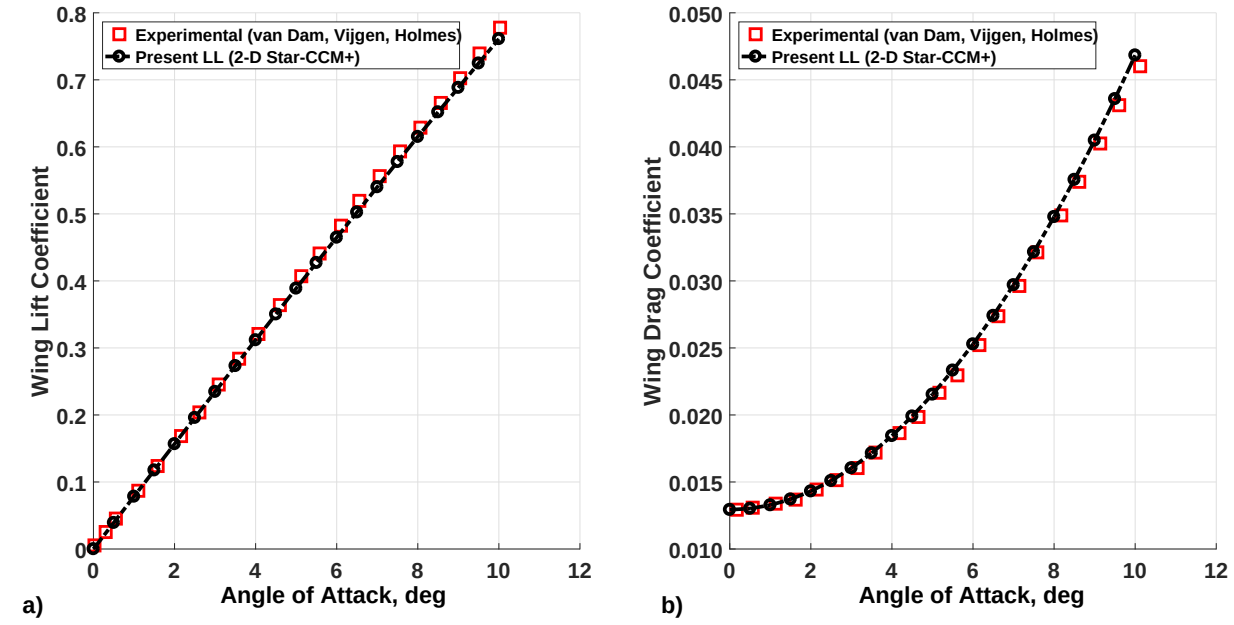

Fig. 13 a) C_L versus α. b) C_D (right) versus α. Elliptical wing (Case IV).

entire α range; the maximum difference for C_L is about 7.0 %, while for C_D is about 8.0 %; the stalled region was not simulated due to the limitations of the nonlinear scheme.

For the $45°-$sweptback wing, $Re_\infty \approx 1.68 \times 10^6$ and $M_\infty \approx 0.15$. The experimental data are from [23]: both lift and drag coefficients were obtained through graphical integration of the pressure measurements along the wing; furthermore,

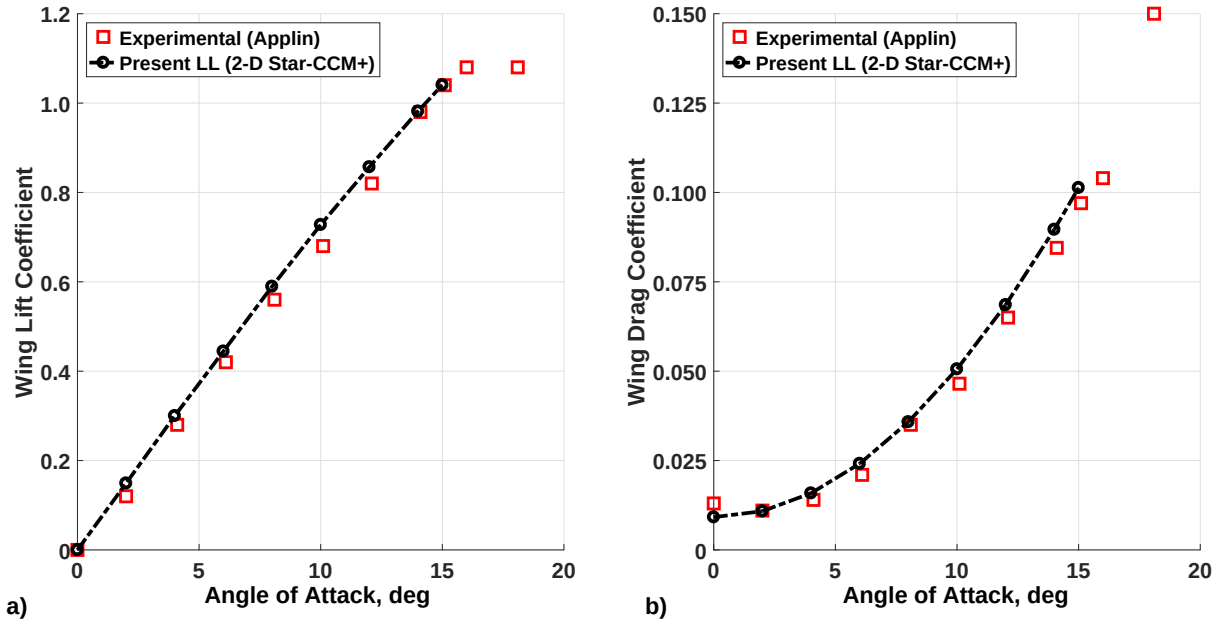

Fig. 14 a) C_L versus α. b) C_D (right) versus α. Straight wing (Case II).

the experiments were conducted until $\alpha \approx 10°$. For the lifting-line, the source of 2-D data was the software XFOIL [26]. In terms of C_L, the agreement is satisfactory for all the α range, a result that sustains the accuracy of the method. In terms of C_D, for low angles of attack, however, the agreement is slightly worse; while there is satisfactory agreement for high angles of attack, for $\alpha \approx 2°$ and $\alpha \approx 4°$ it is not as satisfactory. The maximum differences for both C_L and C_D are about 3.0 % if the lower α region is ignored for the C_D. A previous work had demonstrated the importance of the accuracy of the source of aerodynamic data on the lifting-line, and thus given the possible explanation for such trend [21]: for high α, the predominance is from the induced drag (and thus the close agreement), and as α decreases, the contribution of the viscous drag becomes more substantial, and differences might arise if the 2-D data are not sufficiently accurate due to the suitability of the turbulence models.

As a final validation case, and to demonstrate the capability of the method in simulating swept wings and the influence of viscous effects on lift and drag, a crescent wing with variable sweep throughout the span was simulated (Fig. 16, Case IV). The difference between this wing and the elliptical is the sweep angle distribution; the span, chord at root, inboard section segment, aspect ratio, and arifoil sections are equal. The data are also from [25], and the experimental set-up was kept the same, with the only difference in the placement of the trips to enforce turbulence. Such validation was performed to test the method for a more general chord and sweep distribution.

For the crescent wing, $Re_\infty \approx 2.11 \times 10^6$ with respect to c_0 (or 1.70×10^6 with respect to the mean aerodynamic chord) and $M_\infty \approx 0.27$. The source of aerodynamic data was again Star-CCM+, and it was accounted in the same way as for the elliptical. Although subtly worse than in the elliptical wing, the agreement is still suitable in predicting C_L and C_D, a result that corroborates the appropriateness of the method. The maximum differences for C_L and C_D are about 5.0 %, with the differences increasing with the angle of attack.

VI. Conclusion

A novel wing lifting-line formulation was proposed, in which a nonstandard horseshoe vortex geometry is used. Such geometry was shown to be the most appropriate in terms of stability of the solution and representativeness of the physical assumptions behind the theory. The formulation also uses a nonlinear scheme that incorporates real data from airfoil by approximating the potential and viscous $C_n \times \alpha$ curves through changes in the control points chordwise locations, so the PBC remains satisfied.

Code and solution verification procedures featured the reliability of the proposed method: the solutions converged satisfactorily when a variable chord distribution wing was simulated, when viscous effects were incorporated, and

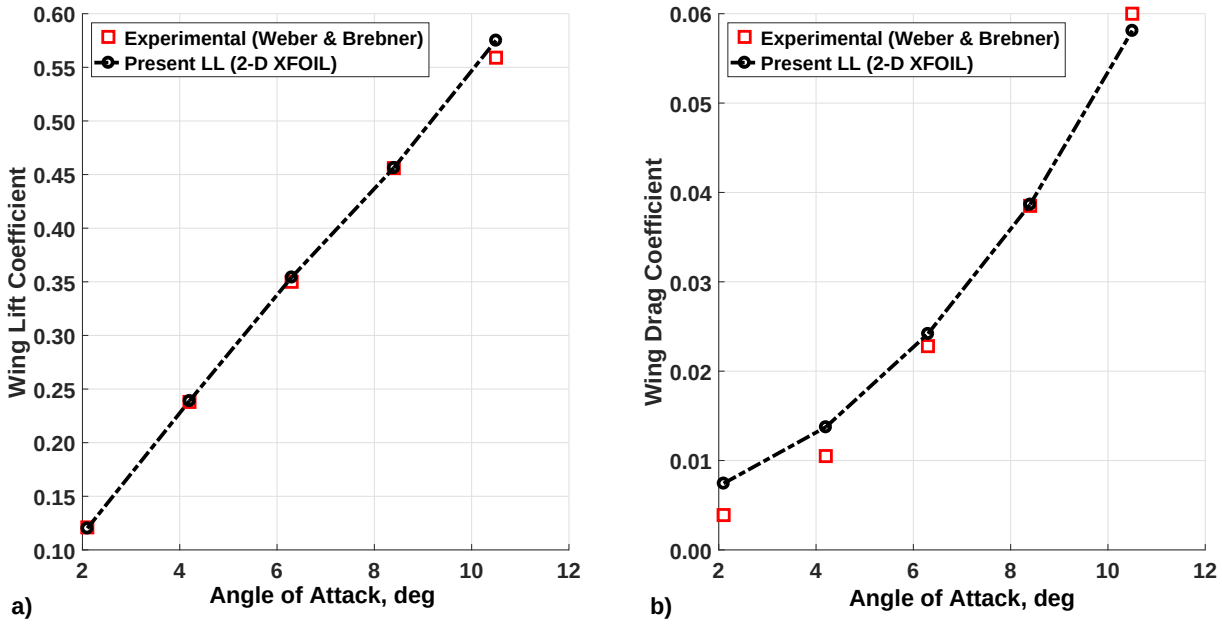

Fig. 15 a) C_L versus α. b) C_D (right) versus α. 45°−sweptback wing (Case III).

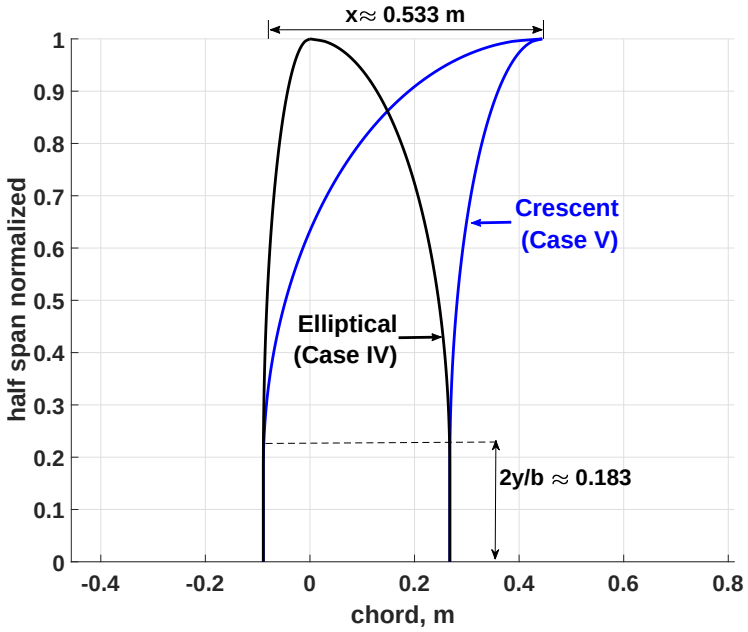

Fig. 16 Planforms of the elliptical and crescent wings used for the validation of the lifting-line method.

when 3-D effects were more prominent. Moreover, three clusterings were evaluated and, while all converged with a satisfactory rate, CHCP presented significantly better results.

Validation against experimental data showed reasonable agreement overall; this confirmed the accuracy of the nonlinear lifting-line in predicting lift and drag for a variety of geometries: an elliptical wing, a straight wing, and a 45°−sweptback were used for validation and the highest relative error was no greater than 7.0% for C_L and 8.0% for C_D. Sequentially, a crescent wing with both variable chord and sweep distributions was simulated and the results also agreed with experimental data to within a small percentage difference.

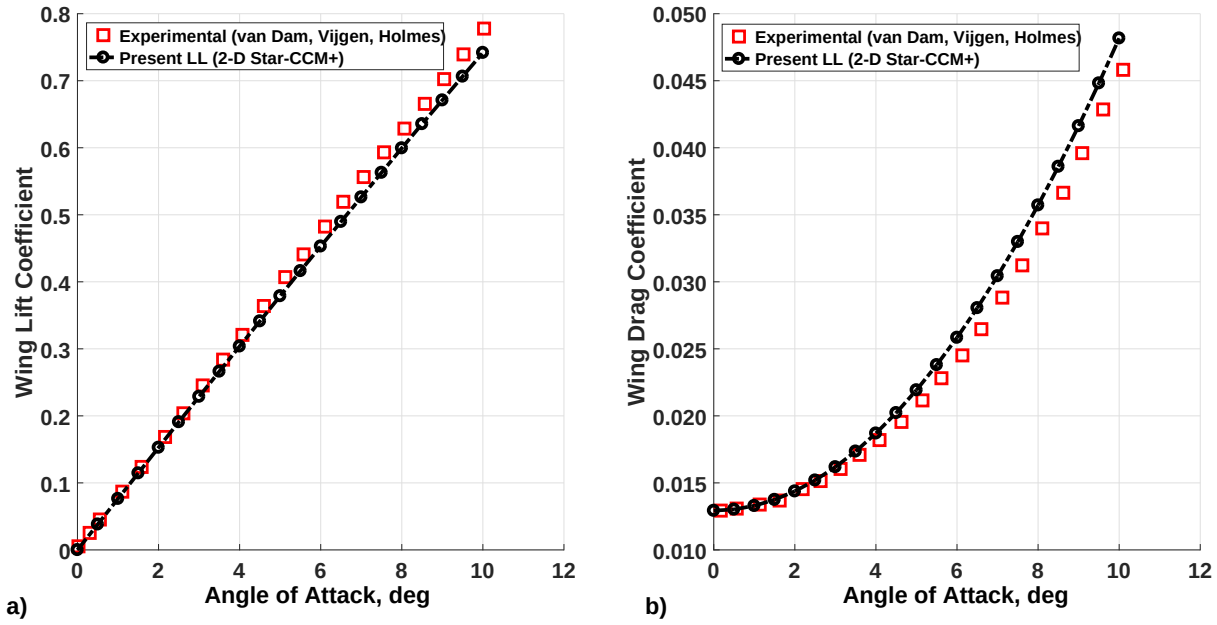

Fig. 17 a) C_L versus α. b) C_D (right) versus α. Crescent Wing (Case IV).

Given the results obtained, the proposed method seems to a good option as a tool for preliminary wing design. As a future work the authors expect to extend the present formulation to the case of propellers.

Acknowledgments

The authors would like to acknowledge the financial support and scholarship granted by the Coordenação de Aperfeiçoamento de Pessoal de Nível Superior (CAPES), under project 1655506, and the Fundação de Apoio ao Instituto de Pesquisas Tecnológicas (FIPT).

References

[1] Bertschneider, H., Bosschers, J., Choi, G., Ciappi, E., Farabee, T., Kawakita, C., and Tang, D., "Final report and Recommendations to the 27th ITTC," *Specialist Committee on Hydrodynamic Noise*, 2014, p. 45.

[2] Anderson Jr, J. D., *Fundamentals of aerodynamics*, Tata McGraw-Hill Education, 2010.

[3] Dragos, L., *Mathematical methods in aerodynamics*, Springer Science & Business Media, 2004.

[4] Weissinger, J., "The lift distribution of swept-back wings," 1947.

[5] Campbell, G. S., "A Finite Step Method for the Calculation of Span Loadings of Unusual Plan Forms," Tech. rep., National Advisory Committee for Aeronautics, 1951.

[6] Anderson, J. D., and Corda, S., "Numerical lifting line theory applied to drooped leading-edge wings below and above stall," *Journal of Aircraft*, Vol. 17, No. 12, 1980, pp. 898–904.

[7] Prössdorf, S., and Tordella, D., "On an extension of Prandti's lifting line theory to curved wings," *IMPACT of Computing in Science and Engineering*, Vol. 3, No. 3, 1991, pp. 192–212.

[8] Barnes, J. P., "Semi-empirical vortex step method for the lift and induced drag loading of 2D or 3D wings," *SAE transactions*, Vol. 106, 1997, pp. 1600–1617.

[9] Owens, D. B., "Weissinger's model of the nonlinear lifting-line method for aircraft design," *36th Aerospace Sciences Meeting and Exhibit AIAA Paper*, Vol. 597, 1998.

[10] Phillips, W., and Snyder, D., "Modern adaptation of Prandtl's classic lifting-line theory," *Journal of Aircraft*, Vol. 37, No. 4, 2000, pp. 662–670.

[11] Chattot, J.-J., "Analysis and design of wings and wing/winglet combinations at low speeds," *42nd AIAA Aerospace Sciences Meeting and Exhibit*, 2004, p. 220.

[12] Wickenheiser, A., and Garcia, E., "Aerodynamic modeling of morphing wings using an extended lifting-line analysis," *Journal of Aircraft*, Vol. 44, No. 1, 2007, pp. 10–16.

[13] Wickenheiser, A. M., and Garcia, E., "Extended nonlinear lifting-line method for aerodynamic modeling of reconfigurable aircraft," *Journal of Aircraft*, Vol. 48, No. 5, 2011, pp. 1812–1817.

[14] Pistolesi, E., "Considerations Respecting the Mutual Influence of Systems of Airfoils," *Collected Lectures of the 1937 Principal Meeting of the Lilienthal Society*, 1937.

[15] Blackwell Jr, J. A., "A finite-step method for calculation of theoretical load distributions for arbitrary lifting surface arrangements at subsonic speeds," 1969.

[16] Gallay, S., Ghasemi, S., and Laurendeau, E., "Sweep effects on non-linear Lifting Line Theory near Stall," *52nd Aerospace Science Meeting*, 2014, pp. 2014–1105.

[17] Pepper, R. S., and van Dam, C., "Design methodology for multi-element high-lift systems on subsonic civil transport aircraft," Tech. Rep. 19960054343, National Aeronautics and Space Administration, August 1996.

[18] Ortega, M. A., Girardi, R. M., and Komatsu, P. S., "A NUMERICAL METHOD TO PREDICT THE LIFT OF AIRCRAFT WINGS AT STALL CONDITIONS," *10th Brazilian Congress of Thermal Engineering and Sciences*, ABCM - Associacao Brasileira de Engenharia e Ciencias Mecanicas, 2004.

[19] de Souza, S. L., "Elaboração de uma Metodologia para predição do Coeficiente de Sustentação Máximo de Asas Flapeadas," Master's thesis, Instituto de Tecnológico de Aeronáutica, 2005.

[20] Katz, J., and Plotkin, A., *Low-speed aerodynamics*, Vol. 13, Cambridge University Press, 2001.

[21] Chreim, J. R., Dantas, J. L. D., Burr, K. P., and Pimenta, M. d. M., "Viscous Effects Assessment Through Nonlinear Lifting-Line Theory," *24th ABCM International Congress of Mechanical Engineering*, ABCM - Associacao Brasileira de Engenharia e Ciencias Mecanicas, 2017.

[22] Committee, V. ., et al., "Standard for verification and validation in computational fluid dynamics and heat transfer," *American Society of Mechanical Engineers, New York*, 2009.

[23] Weber, J., and Brebner, G., "Low-Speed Tests on 45-deg Swept-Back Wings," *Part I, Her Majesty's Stationery Office (HMSO), Reports and Memoranda*, , No. 2882, 1951.

[24] Applin, Z. T., *Pressure distributions from subsonic tests of a NACA 0012 semispan wing model*, Vol. 110148, Citeseer, 1995.

[25] Van Dam, C., Vijgen, P., and Holmes, B., "Experimental investigation on the effect of crescent planform on lift and drag," *Journal of aircraft*, Vol. 28, No. 11, 1991, pp. 713–720.

[26] Drela, M., and Youngren, H., "Xfoil, subsonic airfoil development system," URL http://web. mit. edu/drela/Public/web/xfoil, 2008.